Chapter III.16

Magnets for future colliders: The Muon Collider as a case study

Luca Bottura
CERN, Geneva, Switzerland

The Muon Collider, one of the options considered for the future of particle physics at the energy frontier, poses many challenges to accelerator technology. The magnets for the muon beam production, acceleration and collision are one of the most demanding systems, for many reasons. Firstly, collider performance in terms of energy and luminosity translates in the demand for high fields, high field rates, and large apertures, thus challenging magnet science and engineering well beyond state-of-the-art. At the same time, the operating environment is very harsh: the decay of highly energetic muons, whose products are difficult to shield, results in large heat and radiation loads that need to be managed efficiently. Finally, a muon collider, as any other future collider at the energy frontier, needs to be affordable and efficient to produce sustainable science. The magnets, the single system with the largest cost and power figures, are naturally at the center of the attention also from this point of view. In this note we review the magnet demands and present the conceptual solutions that would meet them. We then expand on the crucial role of high temperature superconductors to meet such challenges. Most interesting, addressing magnet technology challenges for a muon collider will benefit any future collider at the energy frontier, as well as many other fields of scientific and societal application of magnet technology.

III.16.1 Introduction

The Muon Collider (MuC) has been identified as one of the options with great potential for the next step in particle physics at the energy frontier [1]. Muons are point-like particles [2–4] which can be accelerated to very high energies in circular machines since they suffer less from the limitation due to synchrotron radiation experienced by electrons. Studies also show that a MuC with center-of-mass energy of about 1 TeV and higher can provide the most compact and power-efficient route towards a high-luminosity lepton collider [5,6]. The main challenge arises from the short muon lifetime at rest (2.2 µs) and the difficulty of producing bunched beams of muons with small emittance. The main objective for the next years is to evolve from previous ideas and concepts [7,8] towards a consistent MuC concept in the range of 10 TeV center-of-mass energy [9–12]. Normal- and super-conducting magnets have been identified as a crucial technology for a MuC [13]. In fact, the needs of a MuC are such that the desired discovery reach can only be achieved with a significant evolution on several fronts of magnet science and technology. At the same, such advances would positively impact other High-Energy Physics (HEP) options at the energy frontier such as a hadron Future Circular Collider (FCC-hh), as well as (most important) other fields of scientific and societal applications such as magnetically confined thermonuclear

This chapter should be cited as: Magnets for future colliders: The Muon Collider as a case study, L. Bottura, DOI: 10.23730/CYRSP-2024-003.2179, in: Proceedings of the Joint Universities Accelerator School (JUAS): Courses and exercises, E. Métral (ed.),
CERN Yellow Reports: School Proceedings, CERN-2024-003, DOI: 10.23730/CYRSP-2024-003, p. 2179.

fusion, science in high magnetic fields, nuclear magnetic resonance (NMR) and potentially magnetic resonance imaging (MRI). In this chapter we start with a summary of our present understanding of magnet demands, technology options, and concepts, based on the work performed in the scope of the International Muon Collider Collaboration (IMCC) [14]. The layout of the MuC is drawn from US-MAP [7], and is shown schematically in Fig. III.16.1 with all its parts. Although the definition of the various systems is still evolving, the main demands are already clear and stable. We then expand on the advances in specific study cases that represent well the main challenges we identified, and show how a magnet technology based on high-temperature superconductors (HTS) would address and solve many of the challenges.

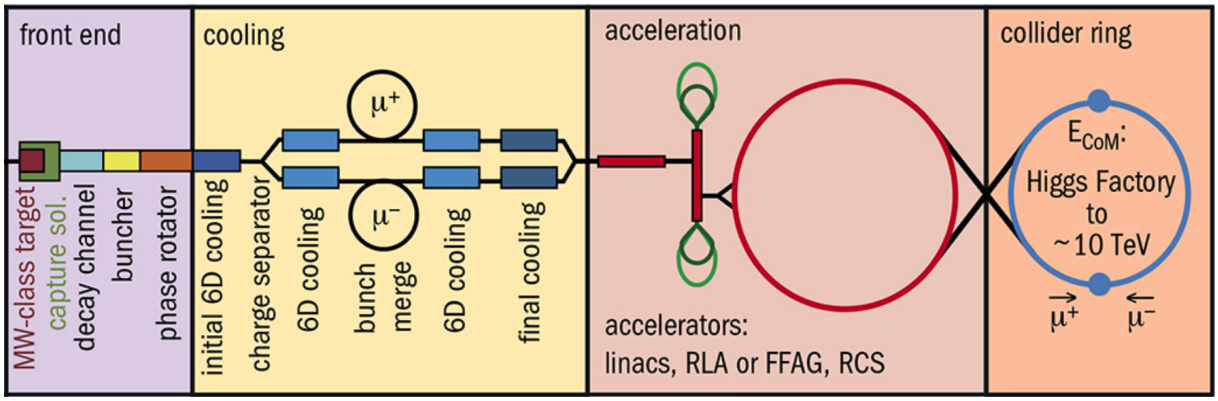

Fig. III.16.1: Schematic layout of the proton-driven Muon Collider, reproduced from Ref. [7]. The proton driver, producing the beam required for muon production, is not shown. The discussion on magnet needs, challenges and conceptual solutions refers to the various parts in the complex.

III.16.2 Magnet needs and challenges

III.16.2.1 Front End (muon production and capture)

Muons beams are produced by the collision of an intense pulsed proton beam with a target of outer dimension in the range of 150 to 250 mm. The proton beam has an energy in the range of 5 to 30 GeV, and an average power of 2 to 4 MW. The proton beam is pulsed, with bunch length of a few ns, and repetition rate of 5 to 10 Hz. The interaction of the proton beam with the target yields muons, pions, kaons, and other secondary particles. Pions and kaons further decay, eventually, in muons. The muons produced directly, and by decay of pions and kaons, have a large momentum and energy spread, i.e. they are a broad cloud of particles moving in different directions at different momenta. To make a small and intense beam of muons requires first capturing them, then reducing the transverse momentum and size of the beam.

This is done by embedding the production target and the following decay and capture channel in a steady-state solenoid, whose function is to bend the charged particles along spirals and guide them towards the exit of the channel. To maximize capture efficiency, the magnetic field profile along the axis of the channel needs to have a specific shape, with peak field of 20 T on the target, and an adiabatic decay[1] to approximately 2 T at the exit of the channel, over a total length of approximately 18 m [15].

[1]We define an adiabatic field decay a variation of the magnetic field over a characteristic length much longer than the gyration

Such a configuration has the property of converting a beam with large transverse momentum and small radius into a beam with smaller transverse momentum but larger physical dimensions. It can thus be used to capture particles produced with a large transverse momentum spread [16].

The solenoids in the target, decay and capture channel are subjected to radiation, caused by the fraction of particles that escape capture. To avoid nuclear heating and radiation damage, the target, decay and capture solenoids need a radiation shield consisting of a combination of a heavy metal like tungsten (to intercept photons from the synchrotron radiation generated by the decay electrons [17]), a moderator like water (to reduce the energy of secondary neutrons), and a neutron absorber (to reduce their fluence). The shield thickness required is in the range of several tens of cm, which effectively defines the magnet bore. Nuclear calculations show that with a shield of approximately 500 mm thickness the radiation heat in the coils would be in the range of 5 kW, local radiation dose in the range of 80 MGy and peak DPA (Displacements Per Atom) in the range of 10^{-2}.

US-MAP envisaged a hybrid super conducting (SC) and normal conducting (NC) solution for the target solenoid, consisting of a large bore low-temperature superconductor (LTS) magnet (approximately 15 T, 2400 mm bore) and a resistive NC insert (approximately 5 T, 150 mm bore) [18–20]. The magnetic energy stored in the system (about 3 GJ), the coil mass (about 200 tons), and the projected wall-plug power consumption (about 12 MW, dominated by the resistive insert) are large. As an alternative, we have proposed a configuration based on a HTS cable operated at 20 K [21, 22]. Figure 2 shows a comparison of the two configurations, the one from US-MAP and the new HTS version we are studying.

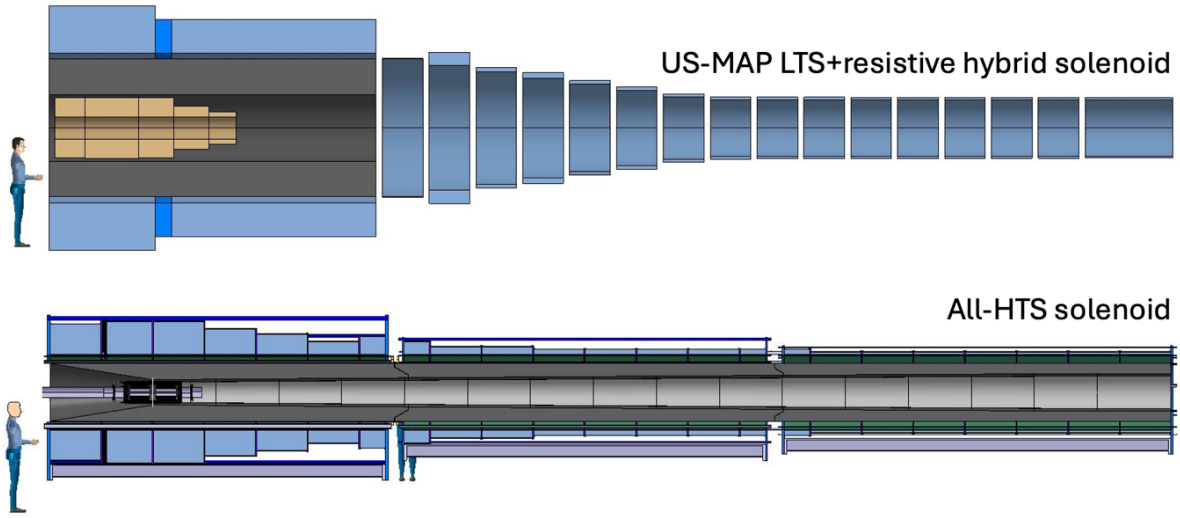

Fig. III.16.2: Comparison (to scale) of the solenoid coils of the target, decay and capture channel of a Muon Collider, as produced by the US-MAP study (top) [20] and resulting from the optimization of an all-HTS solution (bottom) [21]. CAD design by courtesy of A. Kolehmainen, CERN.

The proposed system, shown schematically in Fig. III.16.2, has a stored energy of about 1 GJ, a coil mass of about 100 tons and wall-plug power consumption of about 1 MW, a considerable reduc-

radius of the particles.

tion with respect to the hybrid solution proposed by US-MAP. This demonstrates the potential gain of new magnet technology, and is a good motivation to focus on specific HTS conductor and winding technology suitable for magnets of this class. The main challenge in this proposal is radiation damage of the superconductor and insulation, both requiring further analysis and optimization, measurements, and developments.

The superconducting cable for the solenoids is inspired by the VIPER concept developed at MIT [23], which was validated in short sample tests in the SULTAN facility at Villigen (Switzerland). A copper core with twisted REBCO tapes and a cooling hole is enclosed in a thick steel jacket that provides the main structural support. The cable is shown schematically in Fig. III.16.3, also reporting a view of a mock-up that demonstrates its main features.

Fig. III.16.3: Schematic view of the cable envisaged for the front-end solenoids, showing its main features as well as a mock-up fabricated as a demonstration.

At the operating point of 61 kA, 21 T (peak field) and 20 K, the temperature margin is more than 10 K, which is ample for operation even when considering the radiation heat load. The coil, wound in double pancakes with insulated cable lengths, will require resorting to rad-hard impregnation. The analysis performed so far, also reported in the references given above, shows that it is possible to eliminate the resistive insert and reduce the magnet bore to 1200 to 1300 mm, about half of that of the US-MAP LTS coil, still producing the field profile needed for an efficient muon capture. Operation at temperature higher than liquid helium reduces the need to shield the radiation heat, maintaining good overall energy efficiency. Quench detection and protection can resort on classical techniques of voltage threshold (100 mV) and external energy dump (2.5 kV to ground) to achieve modest hot spot below 150 K [22]. This is also profiting from the low electromagnetic noise associated with steady state operation of the solenoid.

III.16.2.2 Cooling

The beam of muons exiting the target, decay and capture channel has a very large physical dimension and needs to be compacted both in space and momentum to reach dimensions suitable for a collider. This "beam cooling" process is mainly done by a sequence of energy loss steps in an absorber (e.g. liquid H_2

or LiH) where the muons lose momentum in all directions, followed by acceleration in RF cavities where they gain only longitudinal momentum. Similar to what is done in the front end, solenoids placed around the absorbers and RF cavities are used to contain and guide the beam. A km-long sequence of these "6D cooling cells" provides the desired cooling effect in the six dimensions (6D) of the beam phase space (position and momentum).

US-MAP has produced a layout consisting of a total of 826 6D cooling cells, subdivided in twelve types (cells A1 to A4, and B1 to B8) [24,25]. Each cell contains the absorber, an RF module and two, four or six solenoids (depending on the cell) producing the required field profile. We report in Table III.16.1 the main magnet characteristics for the solenoids in the twelve types of cells, and we show in Fig. III.16.4 a synoptic of the field profile in all cells (to scale).

Table III.16.1: Summary of the main solenoid characteristics for the 6D cooling cells of a Muon Collider [24].

Cell	J_E [A/mm^2]	B_{peak} [T]	E_{mag} [MJ]	e_{mag} [MJ/m^3]	σ_{Hoop} [MPa]	σ_{radial} [MPa]
A1	63.25	4.1	5.4	20.5	34	-4.6/00
A2	126.6	9.5	15.4	76.3	137	-28.3/00
A3	165	9.4	7.2	72.8	138	-28.5/00
A4	195	11.6	8.4	91.5	196	-49.4/00
B1	69.8	6.9	44.5	55.9	95	-13.5/00
B2	90	8.4	24.1	61.8	114	-20.1/00
B3	123	11.2	29.8	88.1	174	-36.6/00
B4	94	9.2	24.4	42.4	231	-23.5/19.7
B5	168	13.9	12	86.3	336	-55.7/21.1
B6	185	14.2	8.2	68.3	314	-43.1/22.3
B7	198	14.3	5.7	59.6	244	-37.4/20.7
B8	220	15.1	1.4	20.3	119	-22.9/22.1

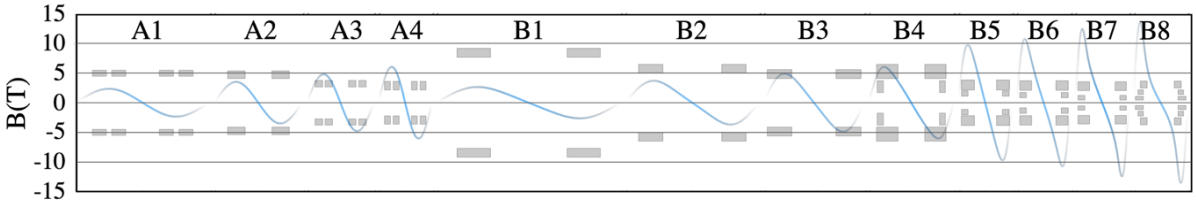

Fig. III.16.4: Collated view of the field profile in the 12 types of 6D cooling cells of a Muon Collider, as resulting from the studies performed within the scope of US-MAP [24]. The corresponding cell type is indicated on top of each segment.

The solenoids in a cell generate a field gradient at the location of the absorber, where the field swings from peak negative to peak positive values, followed by a smoother profile in the RF cavity space. In addition, the peak field tends to increase by moving from upstream to downstream cells. The example of the field generated by the solenoid of a cooling cell is reported in Fig. III.16.5.

We see from Table III.16.1 that the solenoids of the 6D cooling pose several challenges. Although the peak field is not extreme (highest values around 15 T, which is within reach of Nb_3Sn), the stored

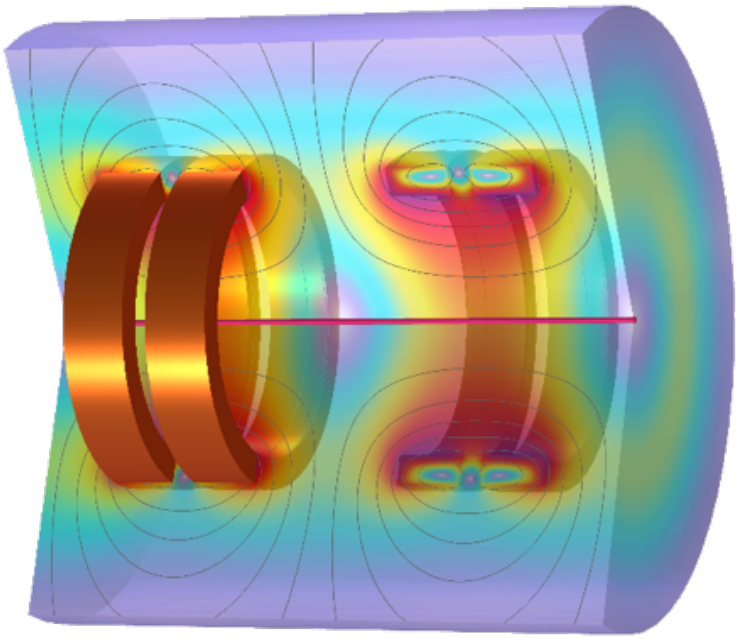

Fig. III.16.5: Field map generated by the solenoids of cell A1, showing the null point in the center of the cell. Design and analysis by courtesy of J. Pavan, INFN, and S.S. Fabbri, CERN.

energy in some of the cells is very large (e.g. cell B1 with 44.5 MJ stored energy). This is an issue for magnet protection, usually managed by winding the coils with cables, to increase the operating current and reduce inductance, and accepting relatively high voltages during a quench. Also at the level of mechanics, the configuration produced will likely require engineering optimization to deal with high hoop (tensile) stresses σ_{Hoop}, with average levels above 300 MPa, e.g. in cells B5 and B6, and the appearance of significant internal tensile radial stresses σ_{radial}, e.g. in cells B4 to B8. Also to be mentioned are the repulsive and attractive forces among coils, in the range of a few MN to tens of MN (e.g. 37 MN in cell B3. Not reported in Table III.16.1). This will pose a challenge to the design of suitable supporting structures, compatible with the integration of room temperature RF cavities and cold absorbers.

The 6D cooling channel is then followed by a "final cooling", where the transverse emittance is further reduced, while the longitudinal emittance grows. Based on linear scaling, the final emittance of the muon beam is inversely proportional to the strength of the final cooling solenoids. The lattice developed in the scope of the design study of US-MAP was based on 17 final cooling cells with solenoids generating fields up to 30 T. The transverse emittance was reduced from an initial value of 45 mm (at the entrance of the 6D cooling channel) to final value of about 55 μm, which is roughly a factor of two greater than the transverse emittance goal of 25 μm [24, 25]. Other analyses [26] have shown that fields in the range of 50 T improve the final emittance and increase transmission, resulting in a brighter final beam.

To improve upon the results obtained by US-MAP we are developing a final cooling solenoid with the potential to reach and exceed 40 T, a clear bore of 50 mm, a length of 500 mm, compact in size to reduce mass, footprint, and, ultimately, also contain cost [27]. At this level of field, the challenge of magnet design is mechanics, because the magnetic pressure associated with the field is at a level comparable with material strength. Taking the simple case of an infinite solenoid with homogeneous current density, we can derive the following relation between the maximum field that can be generated by a solenoid $B_{\max}$ and the peak stress in the coil $\sigma_{\max}$

$$B_{\max} = \sqrt{\mu_0 \sigma_{\max}}, \tag{III.16.1}$$

with μ_0 the vacuum permeability. Taking a maximum allowable stress of 600 MPa as representative of structural material at cryogenic condition, we obtain a maximum magnetic field of about 55 T. This value is only an order of magnitude estimate but gives a good feeling for the challenge at hand.

For the MuC, we are studying a non-insulated (NI) REBCO winding solution, where the cooling solenoid is built as a stack of soft-soldered pancakes wound with a single 12 mm tape (alternative width and multiple tapes are considered). The geometry of the present design is shown schematically in Fig. III.16.6.

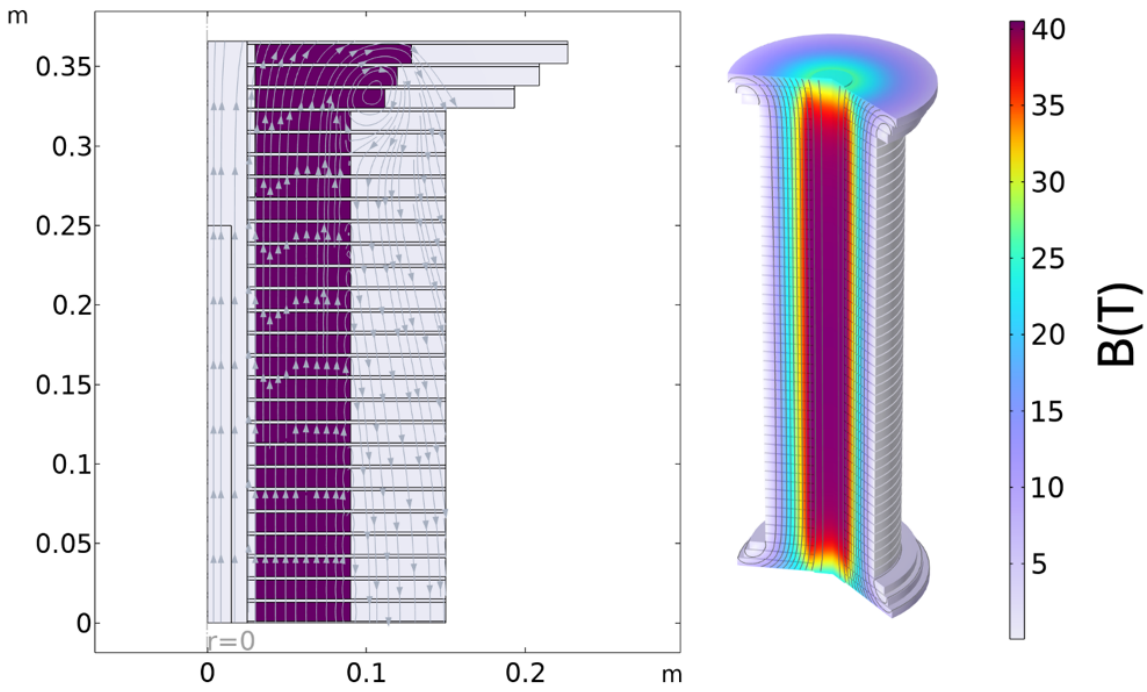

Fig. III.16.6: Schematic of one quarter cross section of the final cooling solenoid for the MuC (left) and magnetic field map (field in T). Design and analysis by courtesy of B. Bordini, CERN.

Given the high field performance required, we have set the operating temperature at 4.2 K. REBCO tapes for use in high field magnets, produced in industry, achieve presently extrapolated values of engineering critical current densities of 250 A/mm^2 in perpendicular 50 T field and 830 A/mm^2 in parallel

50 T field [27]. To reduce the coil size, as well as the forces and stored energy, we target a high operating current density for the central pancakes, in the range of 650 A/mm^2, i.e. less than 50% of critical (considering parallel field). This is within reach of present standard performance, especially considering on-going developments [28].

The resulting coil size is exceptionally small, with a 90 mm outer radius (see Fig. III.16.5). Two critical issues were identified in the conceptual design phase, namely the stress state, already mentioned, and the selection and control of a transverse resistance which needs to be a good balance between the required ramp-rate and quench management. The mechanics of the final cooling solenoid is designed to achieve a maximum Hoop stress of 650 MPa and no tensile stress in any coil powering condition, including quench. This is a must, because industrially produced tapes only tolerate very small tensile and shear stress. At this stage of the conceptual design, we do not consider other structural reinforcements internal to the coil than the tape substrate. The wound and soldered pancakes are loaded in radial direction by a stiff external ring that introduces a radial pre-compression of 200 MPa, at room temperature. This radial pre-compression is crucial to resist the large loads, and is chosen to nearly balance the outward electro-magnetic stress at 40 T. In fact, we have found that this is the field range at which a single pancake reaches the stress limits. Higher fields would require segmenting the coil in concentric and independently-supported layers, adding to the complexity and dimensions.

The stored energy density of the solenoid designed is about 300 MJ/m^3, and the peak temperature in case of uniform quench of the whole solenoid would be a comfortable 200 K. The actual hot-spot temperature depends on the time it takes for the quench to propagate, governed by the electrical and thermal resistance among tapes. For the transverse resistance, our goal is to achieve quench protection through a low transverse resistance (possibly with means to actively trigger quench), while at the same time allowing full ramp in less than 6 hours, as well as field stability at flat-top better than 10 ppm/s. In addition to parametric quench analysis studies, including ideas to improve upon self-protection [29], work is in progress to find means to reduce the values typically obtained when soldering tapes. It is known that most of the current transfer in REBCO tapes takes place through the copper coating of the tape sides, and it was found that reducing or eliminating this part of copper greatly enhances the transverse resistance.

III.16.2.3 Acceleration

Muons need to be accelerated rapidly to extend their lifetime in the laboratory frame. The acceleration consists of a linear accelerator followed by a sequence of a rapid-cycled synchrotron (RCS) and hybrid cycled synchrotrons (HCS) [30, 31]. The RCS is based on NC fast-ramped magnets, swinging from an injection to an extraction field level. In a HCS, static SC magnets provide a field offset, and NC fast-ramping magnets are powered from peak negative to peak positive field, thus making use of a full field swing. This produces an accelerator of smaller dimension than an equivalent RCS. In the present baseline, the NC dipoles in the first RCS need to sweep from 0.36 to 1.8 T within 0.35 ms (i.e. a rate of 4 kT/s). In the last HCS the NC dipoles swing from -1.8 T to 1.8 T, in 6.37 ms (i.e. a rate of about 560 T/s).

An feature of HCS is that because the dipole field variation only takes place in the resistive mag-

nets, the closed orbit in the collider will swing horizontally as shown schematically in Fig. III.16.7. The orbit swing is in the range of 10 to 20 mm, depending on the choice of parameters. This requires that the magnets have wider aperture in the horizontal plane than in the vertical plane, i.e. a rectangular bore.

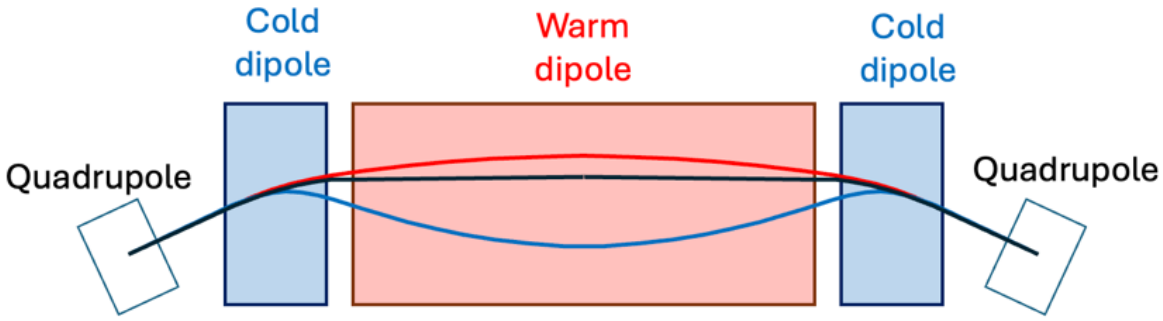

Fig. III.16.7: Schematic view of the orbit oscillations from injection energy (inner orbit, blue) to high energy (outer orbit, red).

Design concepts of NC fast ramped magnets were developed by US-MAP, for peak operating field of 1.5 T [32]. SC dipoles for HCS were not yet studied in detail, besides setting target values for bore field and magnet length. Beyond magnet engineering, the primary challenge of an accelerator ring of the required dimension is that the stored energy is of the order of several tens of MJ (see also later). Powering at a high-pulse rate with good energy recovery efficiency between pulses will require mastery in the management of peak power in the range of tens of GW. Resonant circuits combined with energy-storage systems seem to be the only viable solution [33]. A high energy-storage density and high quality factor are mandatory to limit foot-print, energy consumption, capital and operating cost.

For a specified ramp time and shape, derived from beam design and RF limitations, the power required for pulsing is directly proportional to the magnetic energy stored in the ramped magnets. A lower bound for the stored energy is the magnetic energy in the beam aperture, a nominal 30 mm (gap) $\times$ 100 mm (width). To limit saturation, affecting losses and field quality, we have taken an upper design field limit of 1.8 T for the resistive magnets. This corresponds to a magnetic energy of 3.9 kJ/m in the beam aperture, while the energy stored in the magnet will be forcibly higher. Several resistive magnet configurations shown in Fig. III.16.8, of different iron cross-section and materials, coil design and current density, were analyzed. The result is that the lowest magnet stored energy is in the range of 5.4 kJ/m, a factor 1.4 higher than the magnetic energy in the beam aperture quoted above [34].

A second issue is the magnitude of the resistive, eddy current and hysteresis loss. This is the power drawn from the grid and dissipated. Present estimates are in the range of 500 J/m per pulse, i.e. 10% of the magnetic stored energy. This would result in total resistive losses around 80 MW, which is comparable to the present injector chain of the CERN accelerator complex. Among all configurations analyzed, we have found that the best compromise of stored energy, loss and field quality is obtained with a “H” and “Hourglass” shaped iron core [32].

It is important to remark that the design of the power converter goes hand in hand with the magnet

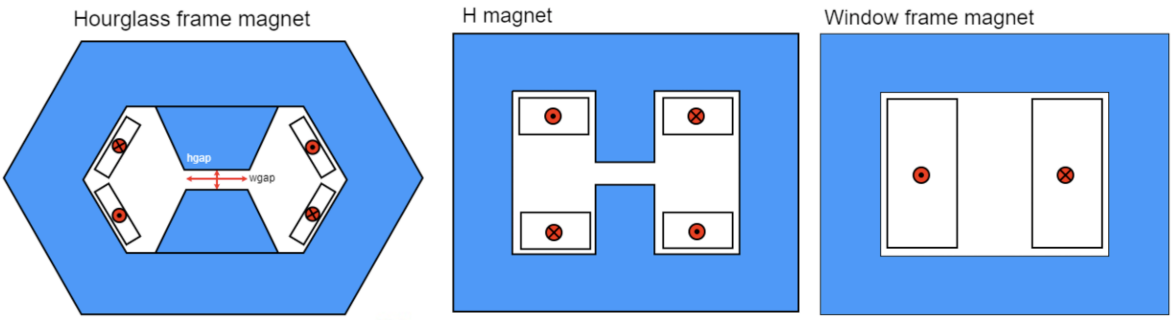

Fig. III.16.8: Cross section of various resistive magnet configurations analyzed. Design concepts by courtesy of M. Breschi, P.L. Ribani and R. Miceli, University of Bologna.

design and analysis, seeking for an optimal cost solution (CAPEX+OPEX) [33], including considerations of beam dynamics and RF. The study of several powering configurations has allowed to identify two main cost drivers, namely the capacitor-based energy storage and the active filters required for the control of the ramp linearity and reproducibility.

The steady-state superconducting magnets of the HCS's are at the level of conceptual design. The specification for these magnets is still in discussion, but the fact that the aperture will be similar to that of the pulsed resistive magnets, i.e. 30 mm $\times$ 100 mm rectangular with large aspect ratio, calls for non-conventional windings. The cos-theta coil geometry customarily used in accelerator magnets is rather inefficient for such a rectangular aperture. A round aperture fitting the rectangular space required by the beam is associated with excess stored energy, material, and cost because of the unused space. This is why we have directed conceptual work towards flat racetrack coils, simple and suitable for winding with HTS tapes. It seems that it may be possible to achieve a field target around 10 T, at an operating temperature significantly above liquid helium in case HTS is used (10 to 20 K). This would be highly beneficial to cope with operating margin and efficiency requirements in HCS's, which tend to be rather "dirty" machines as far as beam losses are concerned. Initial configurations considered for the steady state SC magnets are shown in Fig. III.16.9.

The concept development for these magnets is only at the beginning, but because of steady state operation, it may be possible to use also in this case a NI winding with benefits for quench protection. In fact, the concept of superconducting HCS magnet suggested above resembles closely on-going developments at associated laboratories [35].

Besides the use as steady bending magnets in the HCS stages, HTS magnets are also considered as an alternative for the pulsed dipoles in the last synchrotron. This stage requires ramp-rates of about 500 T/s, close to values recently demonstrated in a super-ferric dipole achieving a field of 0.3 T at 300 T/s [36]. The challenge is to demonstrate that fields of the order of 2 T, or higher, can be reached with acceptable AC loss.

III.16.2.4 Collider

The last stage of the muon accelerator complex is the collider ring, where two counter-rotating positive and negative muon beam bunches collide. The collider ring needs to have the smallest possible circum-

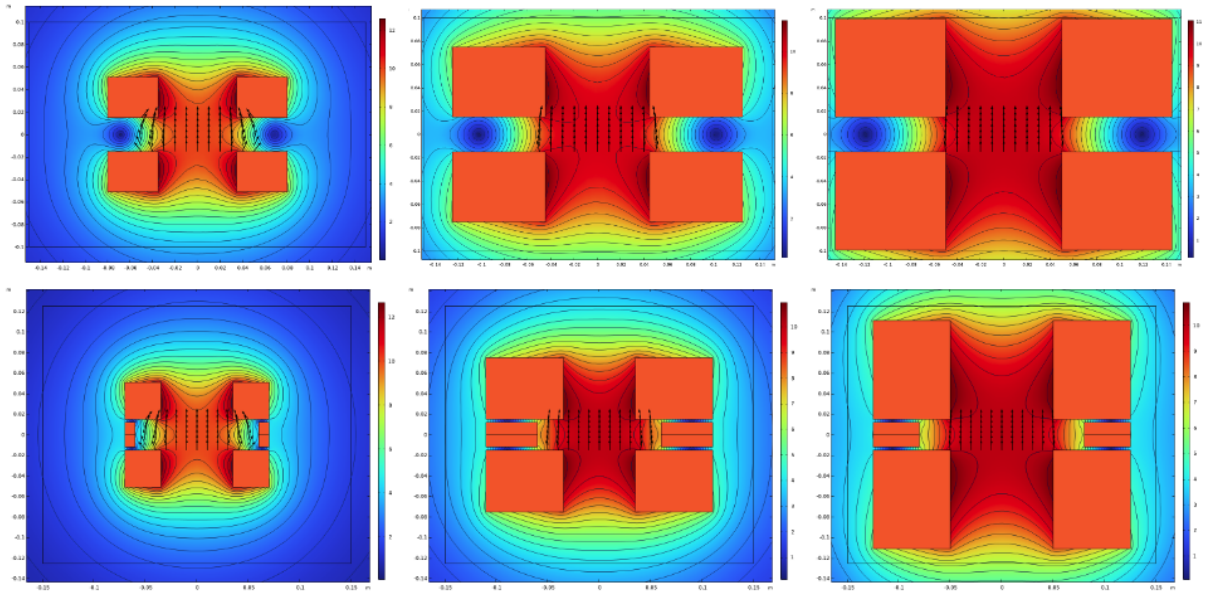

Fig. III.16.9: Cross section of various superconducting racetrack magnet configurations analyzed, all producing 10 T in the rectangular bore, but improved field quality (from left to right) and higher magnetic efficiency (bottom vs. top). Designs and analyses by courtesy of S.S. Fabbri, CERN.

ference to collide the stored muon beams as often as practically feasible and thus make the best use of their limited life-time [37]. This implies that the dipoles needs to generate the highest feasible and practical field. At the same time, sufficient radiation shielding must be present to protect against the sizeable radiation and heat loads from muon decay and collisions. The heat load of 500 W/m originated by muon decay (electrons) and synchrotron radiation is reduced by shielding (30 to 40 mm) to values in the range of 5 to 10 W/m at the level of the coil, and radiation dose below 40 MGy [17]. The presence of such thick shield makes the magnet aperture forcibly large. The arc and Interaction Region (IR) dipole and quadrupole magnets thus need to be high-field and large aperture, as studied in Refs. [38, 39].

The assumptions for the present study of the 10 TeV collider optics are rather aggressive. The assumption is that the main arc magnets generate a steady-state magnetic field up to 16 T in a 160 mm aperture. To reduce straight sections, and mitigate the effects from the high neutrino flux, the arc magnets are presently assumed to have combined functions (e.g. dipole/quadrupole and dipole/sextupole) [37]. For the IR quadrupole magnets the assumption from the optics studies is of a peak field of 20 T, also associated with large apertures, up to 300 mm. Dipole fields are in the range of 10 to 16 T and gradients in the range of 100 to 300 T/m are demanded.

To understand how to design for such challenging performance, we have established performance limits of accelerator dipole and quadrupole magnets by using analytical methods [40]. The basic assumption is that the coil geometry is a sector. The conditions to be satisfied are

- An operating margin of about 2.5 K, based on a minimum enthalpy margin and considerations of temperature stability in the magnet;
- Peak stress below the coil and conductor degradation limit, taken equal to 100 MPa for Nb-Ti,

150 MPa for Nb_3Sn, and up to 400 MPa for REBCO;

– A maximum hot-spot temperature, set to 300 K for Nb-Ti and Nb_3Sn, and 200 K for REBCO;
– An upper magnet cost per unit length of 400 kEUR/m, based on aspirational cost figures for the superconductor of about one third of present cost.

The results are specific to the sector coil geometry, but extension to other coil geometries is possible and will not significantly change the main outcome. Though the analytical evaluations discussed above are not intended as a magnet design, they provide much required guidelines towards the selection of suitable design points for the collider ring and IR optics.

We have used the analytical evaluation to produce design charts of maximum magnet aperture (A) vs. bore field (B), which is a form convenient for iterating with the beam optics. Such A-B charts were produced for a choice of superconductor and operating point of Nb-Ti at 1.9 K, Nb_3Sn at 4.5 K and REBCO at 20 K. A sample of such plots is shown in Fig. III.16.10 [40].

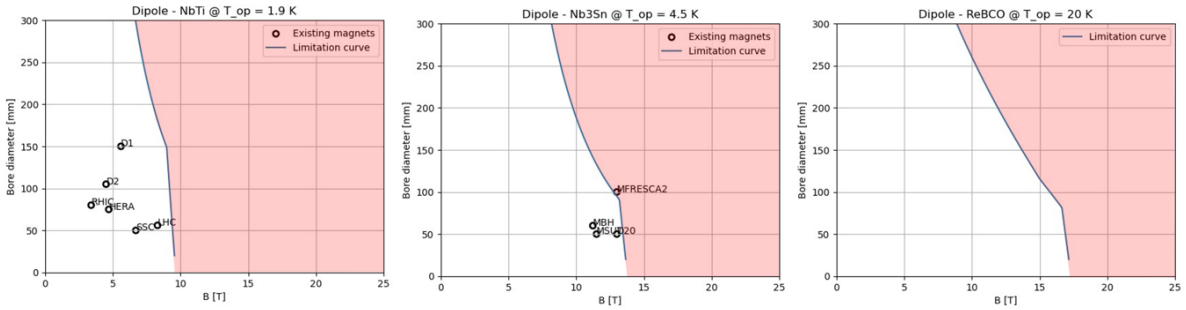

Fig. III.16.10: A-B plots generated for dipoles built with Nb-Ti, Nb_3Sn and REBCO. Also indicated dipole magnets that have been built with Nb-Ti, Nb_3Sn and tested [40]. Analysis by courtesy of D. Novelli, S. Mariotto and B. Caiffi, INFN.

For a 10 TeV collider, Nb-Ti at 1.9 K does not appear as a good solution because of low operating margin (recall the large energy deposition), as well as considerations of cryoplant efficiency and energy consumption. Similarly, Nb_3Sn at 4.5 K falls short of the required field performance for the arc magnets, providing feasible solutions only up to 14 T. The operating margin, based on an enthalpy margin of 20 mJ/cm^3 as for the HL-LHC magnets and resulting in a temperature margin of 2.5 K, results in a hard limit to the performance of Nb_3Sn magnets with a material amount below the set cost allowable of 400 kEUR/m. In addition, setting a maximum allowable transverse stress of 150 MPa yields to a maximum aperture of about 100 mm at the peak field reached, far from the 160 requested. Quench protection in this range of field and aperture seems feasible with standard detection and protection techniques.

Our initial evaluation of REBCO shows that also in this case the available design space does not match the required performance. For REBCO, however, operating margin is not an issue, and operation in the range of 10 to 20 K could be envisaged, still allowing for a temperature margin of 2.5 K. This has a great benefit for the power consumption, potentially reducing the wall-plug power of the cryoplant by a factor two to four. Mechanics is also no longer the most stringent limit, provided one can profit from the good resistance of tapes to transverse stress (data shows single tape withstand up to 400 MPa with no degradation). The main limitations come rather from quench protection, associated with the

cost of the superconductor. Cost considerations drive the current density in an all-HTS coil towards high values, in the range of 800 to 1000 A/mm^2, where standard detect-and-dump protection strategies are not sufficiently fast. It is hence clear that alternative protection schemes need to be devised to benefit from the large critical current and margin of present REBCO conductors.

Provided that the cost per meter of REBCO tape can be reduced by a factor of about three, relaxing the need for very high values of current density, we have found that a suitable design range for the arc magnets can be defined using two points, from a nominal aperture of 160 mm at reduced bore field of 12 T, up to nominal bore field of 16 T but reduced aperture of 100 mm. The whole range can be achieved with REBCO at 20 K, while the low field range can be reached also with Nb_3Sn at 4.5 K, thus providing at least two technology options. In addition, REBCO at 10 to 20 K would be compatible with larger energy deposition in the coils, i.e. reduced shielding and smaller magnet aperture. A simple evaluation based on radiation studies shows that a 10 mm reduction in shielding thickness (20 mm in aperture) may be possible, with no penalty on wall-plug power, still at acceptable levels of radiation damage.

III.16.3 Summary of magnet performance targets

To give a summary of the magnet challenges for a muon collider, we report in Table III.16.2 the main performance targets and target ranges (i.e. not yet a specification) for the most challenging magnets of the MuC. They identify what we consider a feasible magnet performance range within the time scale of construction of a MuC. Though these targets are bound to adapt as the MuC study proceeds, they already provide a good basis to feedback on beam optics and accelerator performance, and to identify outstanding issues to be addressed by future work and dedicated R&D.

Table III.16.2: Summary of magnet development targets.

Complex	Magnet	Aperture [mm]	Length [m]	Field [T]	Ramp-rate [T/s]	Temperature [K]
Front-End	Solenoid	1200	19	20	SS	20
6D cooling	Solenoid	90–1500	0.08–0.5	4–15	SS	4.2–20
Final cooling	Solenoid	50	0.5	> 40	SS	4.2
Final cooling	NC dipole	30×100	5	± 1.8	500–4200	300
RCS	SC dipole	30×100	1.5	10	SS	4.2–20
Collider ring	dipole	160–100	4–6	12–16	SS	4.2–20

III.16.4 Conclusions—the role of HTS

It is clear from the previous discussion, as also signified by the targets of Table III.16.2, that HTS have a main role in addressing the challenges of the MuC. There are several reasons for this.

The first, and most immediate reason, is that HTS materials have the potential to take accelerator magnets to the next level in terms of field and aperture. HTS have exceptionally high critical fields, as shown in Table III.16.3 and Table III.16.4, where we report the main properties of state-of-the-art technical superconducting materials (i.e. produced in industry). With critical fields in the vicinity, or more than 100 T, HTS can carry current at field levels well above LTS materials, where the limitations are no longer the critical properties, as we have already recalled earlier. This opens a new design space,

which is useful for future colliders to reach higher fields in all magnet types: solenoids, as well as accelerator dipoles and quadrupoles.

Table III.16.3: Technical superconducting materials (LTS) and their critical properties.

Material	Nb-Ti	Nb_3Sn	Nb_3Al	MgB_2
Discovery year	1961 [41]	1954 [42]	1958 [43]	2001 [44]
T_c [K]	9.2	18.2	19.1	39
B_c [T]	14.5	~ 30	33	36–74

Table III.16.4: Technical superconducting materials (HTS) and their critical properties.

Material	YBCO	BSCCO	IBS
Discovery year	1987 [45]	1988 [46]	2008 [47]
T_c [K]	~ 93	95 (2212 phase) 108 (2223 phase)	55
B_c [T]	~ 120 (B // c-axis) ~ 250 (B // ab-plane)	~ 200	70 (IBS-122)

HTS materials, and in particular REBCO, tend to have a varying degree of critical current anisotropy, factors three to five at high field, and come in tape form, which is a disadvantage to form flexible cables. But they are either deposited on sturdy substrates, or can be co-laminated to reinforce them. This is important because stresses and strains are design drivers for high field magnets, and all superconductors for high field applications (LTS and HTS) are brittle. Finally, the stability of HTS materials resolves the issue of magnet training, but makes quench detection and protection significantly more difficult than in LTS. Non-insulated windings can provide a solution, ideally making the magnets self-protecting.

The second reason of the growing interest for HTS is the fact that the efficiency of a cryogenic installation tends to increase as the temperature of the cold end increases. This general statement is usually justified by looking at the efficiency of an ideal reversed Carnot cycle, which we can write as follows [48]

$$\eta_{\text{Carnot}} = \frac{T_{\text{Cold}}}{T_{\text{Hot}} - T_{\text{Cold}}}, \tag{III.16.2}$$

where T_{Cold} is the temperature at the cold end, removing heat, and T_{Hot} is the temperature at the warm end, where the heat is rejected. Taking an operating temperature T_{Cold} in the range of 4.2 to 20 K, where HTS can produce fields up to 20 T, and a warm end at T_{Hot} of 300 K, we see that the Carnot efficiency is nearly five times better at 20 K than at 4.2 K. In reality, cryogenic fluids are far from being ideal gases, and cryogenic cycles are far from being reversible. The efficiency of real cryogenic machines is customarily characterized by a Coefficient of Performance (COP), defined as

$$\text{COP} = \frac{Q_{\text{Cold}}}{P_{\text{Hot}}}, \tag{III.16.3}$$

where Q_{Cold} is the power removed at the cold end, and P_{Hot} is the power required to run the cryogenic machine. Because of the above reasons, we always have COP $\leq \eta_{\text{Carnot}}$. The ratio of efficiency depends, among others, on characteristic parameters of the machine such as cold-end power Q_{Cold} and temperature T_{Cold}. To give relevant orders of magnitude we report in Fig. III.16.11 the inverse of the COP, i.e. the warm power required to remove a given cold power. The line corresponds to the Carnot efficiency, while the points are cryogenic machines that have been built and operated in accelerators, with cold power range from 3 to 30 kW.

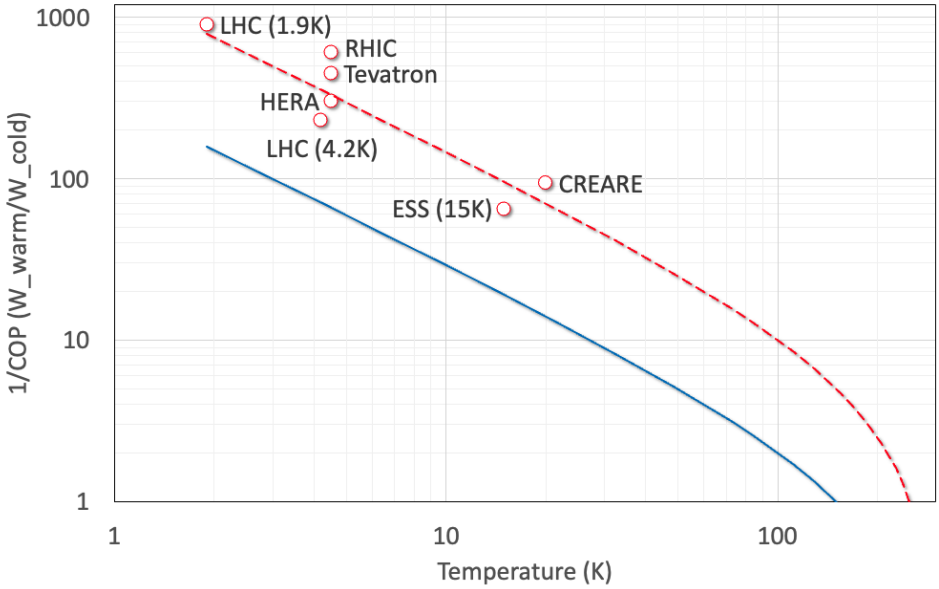

Fig. III.16.11: Inverse COP derived from the Carnot efficiency (blue line) and as measured in cryogenic machines that have been built and operated in accelerators. The dotted line is a guide to the measured COP.

We see that the warm power required in real machines is, as expected, significantly larger than that of an ideal Carnot cycle. The factor is from three (best case of LHC 18 kW refrigerators at 4.2 K) to five (average fit), and this is a known effect. What is also interesting though is the confirmation that there is a significant gain, a factor four, in increasing the operating temperature from 4.2 K to 20 K as can be made possible by using HTS materials.

A second benefit of an increased operating temperature made possible by HTS is the fact that the thermal management becomes easier. Requirements on thermal shields, vacuum levels and tolerances are relaxed, thus facilitating the construction of the magnet systems in their cryostats.

The third reason for the great interest in HTS is economics, namely the potential for cost reduction. Future colliders at the energy frontier are likely to be significantly larger, or more performant, or both, when compared to the state of the art. The most flagrant examples are the FCC [49], or the CEPC/SppC [50–52], with tunnel lengths in the range of 100 km and dipole magnets in the range of 14 to 20 T. Technology progresses hand-in-hand with demands from physics, decreasing the specific cost of the technical infrastructure of accelerators as shown in Fig. III.16.12, from Ref. [53]. Note that we plot there the specific cost per parton center-of-mass energy of the collision (pCOM), assuming a simple fac-

tor seven for the equivalence between protons and leptons. From the figures plotted there, it is expected that the next step at the energy frontier, projected in the range of 10 TeV pCOM energy, should reach a specific cost of 1 MCHF/GeV, corresponding to a target cost of 10 BCHF, which is very close to the cost estimate of the magnet system of the FCC-hh [54]. For an FCC-hh, with a tunnel length of 91 km and a filling factor of 80% this corresponds to a cost per magnet unit length of approximately 90 kCHF/m. We note that the present cost of Nb_3Sn HL-LHC magnets is approximately 480 kCHF/m[2], i.e. over five times larger than desired [55]. Something needs to be done.

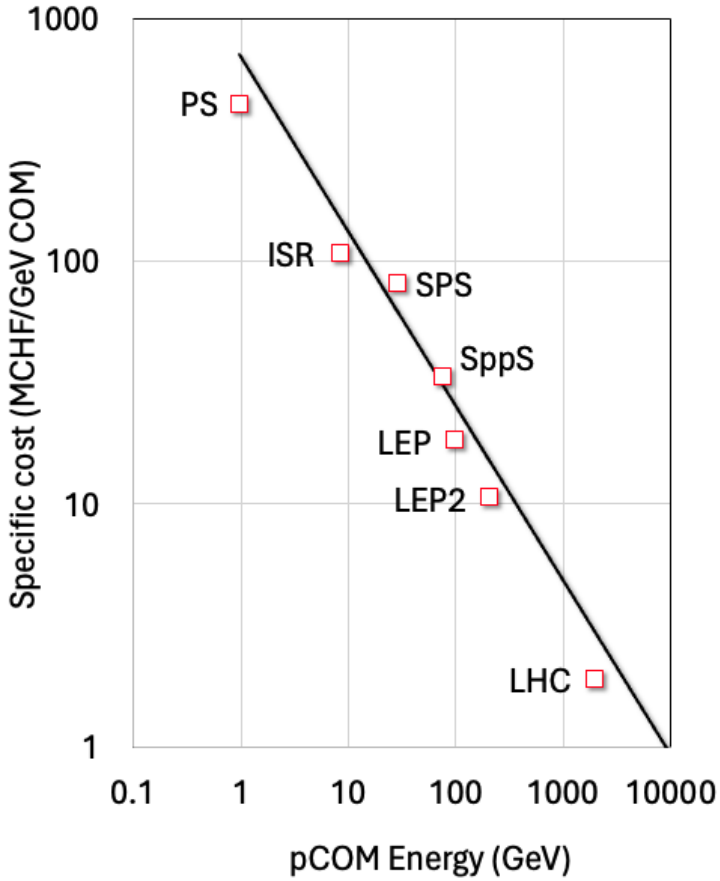

Fig. III.16.12: Specific cost of technical systems, referred to the parton center of mass energy, for all colliders built at CERN. Reproduced from Ref. [53].

HTS has the potential to reduce the cost of future magnets in two ways. On one side the spectacular critical current properties can be exploited to build coils that operate at engineering current density higher than LTS, thus reducing the amount of expensive superconducting material used. This is a natural trend that has been observed throughout the history of the superconducting collider, as shown in Fig. III.16.13 that reports the engineering current density in the dipole magnets from the beginning of the Tevatron to the present High Luminosity LHC magnets. This trend can be understood easily when looking at the

[2]The cost is estimated based on the HL-LHC magnet production, excluding R&D and tooling, taking the 2019 present prizes for superconductor, other materials, consumables and labor and adjusting for a 20% cumulated inflation in the five years period 2019–2024.

dipole field generated by a sector magnet of uniform coil current density J and (inner) bore radius R_{in}

$$B = \frac{2\,\mu_0}{\pi}\,J\,w\,\sin\phi \quad , \tag{III.16.4}$$

where w is the coil width and ϕ is the pole angle. If we fix a given dipole field B, the cross section of the coil A_{coil} that produces that field scales like

$$A_{\text{coil}} = 2\,\phi\,(w^2 + 2\,R_{\text{in}}\,w) \sim \frac{1}{J^n} \quad , \tag{III.16.5}$$

where n is an exponent ranging from 1 to 2, and in the range of dimensions of typical dipoles (10–20 T field, 50–150 mm aperture, 15–60 mm coil width) it is approximately 1.3. In fact, we see in Fig. III.16.13 that the engineering (coil) current density has nearly doubled since the initial values of the Tevatron and HERA (295 A/mm2) to the present values of the 11 T dipoles for HL-LHC (520 A/mm2). This translates in a reduction by factor 2.5 in the coil cross section required to generate a given field, a significant gain in cost. This trend is likely to continue in the future, but this will only be possible resorting to HTS, and exploiting new coil technology such as non-insulated windings to overcome mechanical and quench protection limits.

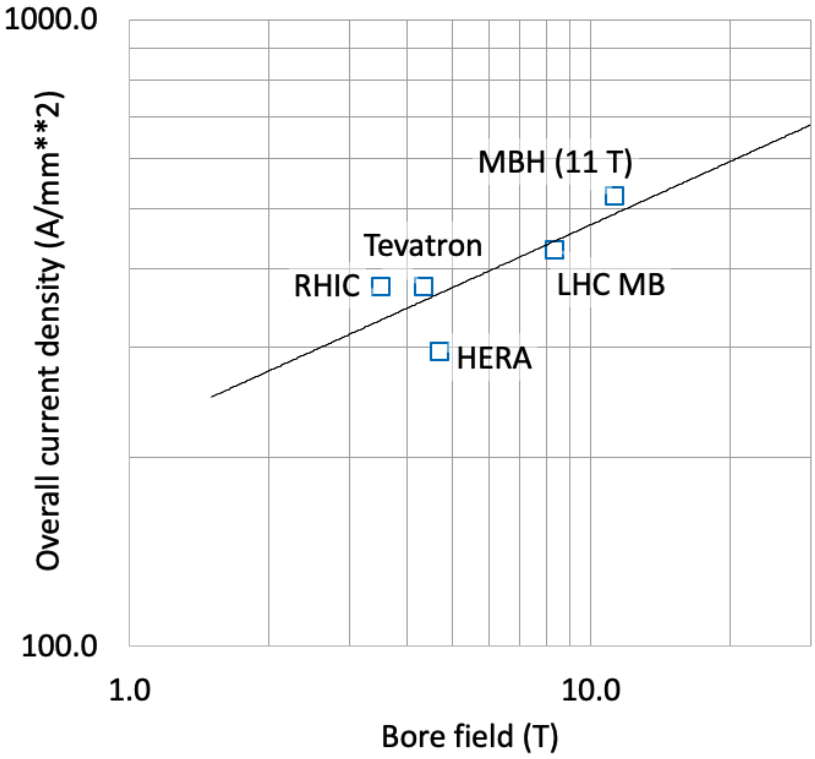

Fig. III.16.13: Engineering current density (coil) of the collider dipole magnets built to date.

At the same time, HTS also has great potential for a reduction of the unit cost of the superconducting material. As shown by Ref. [56], the cost of a superconductor can be obtained from the cost of raw materials, applying a multiplier P that depends on the complexity, maturity and scale of the manufacturing process. The typical value of P for Nb-Ti is 3, indicating a mature and relatively simple process,

used for the production in large scale (several thousand tons per year). For Nb_3Sn the present value of P is rather around 10, with potential for some reduction, up to a factor three. The issue is that the present production of Nb_3Sn remains relatively small, with no perspective for a significant boost, even in the case of production for a next step collider. It is hence unlikely that the cost of Nb_3Sn will decrease significantly, similarly to what seen in the case of the production of 600 tons of wire for ITER. For HTS, on the other hand, P is greater than 100. While this the result of the complexity of the process, it also points to the potential for a significant cost reduction [57]. This is exactly what we have witnessed with the procurements at CERN in the last fifteen years, reported in Fig. III.16.14, a trend mainly driven by the demand originating from R&D on compact thermonuclear fusion devices. We have plotted there the cost per unit length and unit current carried by the superconductor, for Nb_3Sn and HTS (mainly REBCO). The actual cost has been scaled to yield arbitrary units and avoid disclosing financial offers. We have chosen to compare normalized costs at a field of 12 T and at a temperature of 4.2 K, the typical range where Nb_3Sn is expected to have a leading edge. Finally, trendlines are only reported to guide the eye, they are not indicating expected evolution.

Despite all caveats, it is very suggestive that HTS costs per unit current are approaching those of Nb_3Sn, fast. Even today, at 12 T and 4.2 K, the best normalized HTS cost is not far from that of Nb_3Sn. Had we taken 16 T as the benchmark field, the normalized cost of HTS would be well below that of HEP-grade Nb_3Sn. Many issues of magnet technology need to be resolved, but this analysis clearly points to the need for a focused effort in making HTS accelerator magnets a reality.

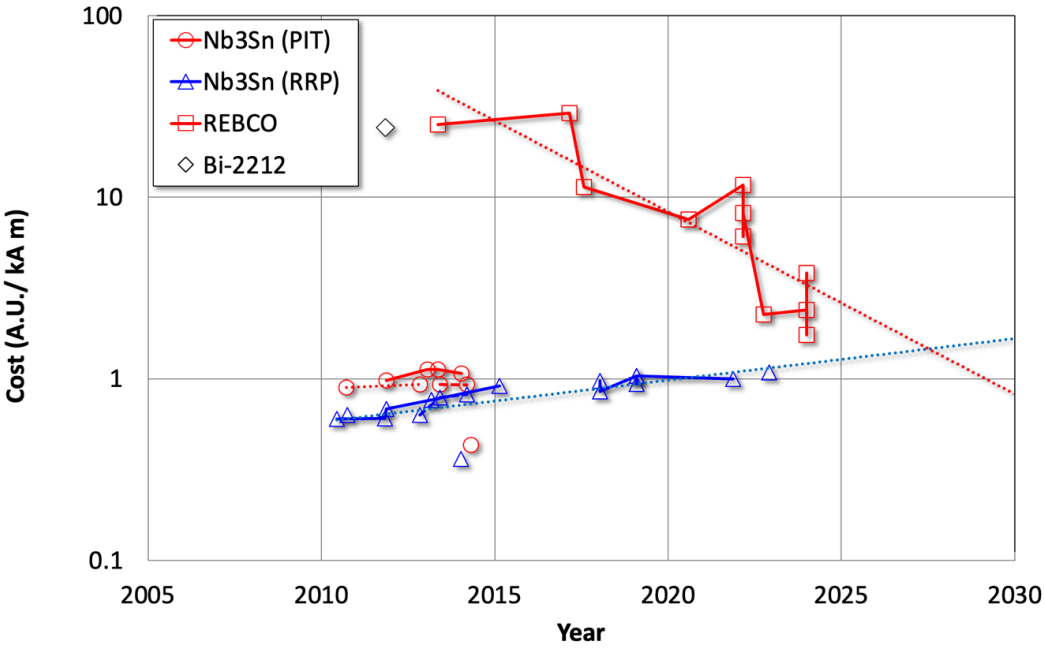

Fig. III.16.14: Cost (arbitrary units) per unit length and current for Nb_3Sn and HTS (mainly REBCO), derived from purchases at CERN in the last fifteen years. The normalization is done for a field of 12 T and an operating temperature of 4.2 K.

Finally, a last and most important reason for the interest in HTS, is that HTS magnet technology has many overlaps with other fields of magnet science. This is a very strong motivator for present and

future research and development with relevance to other scientific and societal applications such as

- Magnetically confined thermonuclear fusion;
- High magnetic field science;
- UHF magnets for nuclear magnetic resonance and research in magnetic resonance imaging;
- Fast ramped magnets for radiation therapy;
- Compact planar and non-planar coils for superconducting motors and generators.

In conclusion, a MuC at the energy frontier depends critically on HTS magnet technology. At the same time, the HTS magnet technology developed for a MuC would greatly impact other fields of scientific and societal applications, including any future collider such as the FCC and the SppC. It is exactly this virtual circle that has fueled magnet technology for HEP in the past fifty years, which we wish to foster and nourish.

III.16.5 Acknowledgements

The work reported in this article is the fruit of the intense collaboration running within the scope of the International Muon Collider Collaboration and partially funded by the EU through the MuCol design study (Grant Agreement N° 101094300). Besides the references to the material reported, we especially wish to acknowledge the contributions of S.S. Fabbri and F. Boattini (CERN), M. Statera and S. Mariotto (INFN-Milano), B. Caiffi (INFN-Genova).

References

[1] M. Boscolo, J.P. Delahaye, and M. Palmer, “The future prospects of muon colliders and neutrino factories,” Reviews of Accelerator Science and Technology, vol. 10, no. 01, pp. 189–214, 2019, doi:10.1142/9789811209604_0010.

[2] C. Aimè, A. Apyan, M. A. Mahmoud, N. Bartosik, et al., “Muon collider physics summary,” FNAL Report FERMILAB-PUB-22-377-PPD, 2022, doi:10.48550/arXiv.2203.07256.

[3] D. Stratakis, N. Mokhov, M. Palmer, N. Pastrone, et al.,“A muon collider facility for physics discovery,” 2022, doi:10.48550/arXiv.2203.08033.

[4] J. de Blas, et al., “The physics case of a 3 TeV muon collider stage”, FNAL Report FERMILAB-CONF-22-317-AD-ND-PPD-SCD-TD, doi:10.48550/arXiv.2203.07261.

[5] K. Long, et al., “Muon Colliders: Opening New Horizons for Particle Physics”, Nature Physics, v.17, p.289, 2021, doi:10.1038/s41567-020-01130-x.

[6] D. Neuffer and V. Shiltsev, “On the feasibility of a pulsed 14 TeV c.m.e. muon collider in the LHC tunnel”, 2018 JINST 13 T10003, doi:10.1088/1748-0221/13/10/T10003.

[7] R. Palmer,“Muon colliders,” Reviews of Accelerator Science and Technology, vol. 7, pp. 137–159, 2014, doi:10.1142/S1793626814300072.

[8] M. Palmer, “The US muon accelerator program,” FNAL Report FERMILAB-CONF-14-346-APC2015, doi:10.48550/arXiv.1502.03454.

[9] D. Schulte, "The International Muon Collider Collaboration," in Proc. IPAC'21, pp. 3792–3795, JACoW Publishing, Geneva, Switzerland, doi:10.18429/JACoW-IPAC2021-THPAB017.

[10] European Strategy Group, "2020 Update of the European Strategy for Particle Physics," tech. rep., Geneva, 2020, doi:10.17181/CERN.JSC6.W89E.

[11] "European Strategy for Particle Physics - Accelerator R&D Roadmap", N. Mounet (ed.), CERN Yellow Reports: Monographs, CERN-2022-001 2022, doi:10.23731/CYRM-2022-001.

[12] MuCol - A Design Study for a Muon Collider complex at 10 TeV center of mass, EU Grant Agreement 101094300, doi:10.3030/101094300.

[13] L. Bottura, et al., "A Work Proposal for a Collaborative Study of Magnet Technology for a Future Muon Collider", 2022, doi:10.48550/arXiv.2203.13998.

[14] C. Accettura, "Towards a Muon Collider", The European Physical Journal C, 83, 864, 2023, doi:10.1140/epjc/s10052-023-11889-x.

[15] H.K. Sayed and J.S. Berg, "Optimized capture section for a muon accelerator front end", Physical Review Special Topics-Accelerators and Beams, vol. 17, 070102, 2014, doi:10.1103/PhysRevSTAB.17.070102.

[16] P. Royer, "Solenoidal Optics", CERN-OPEN-2000-324, 1999.

[17] D. Calzolari et al., "Radiation Load Studies for Superconducting Dipole Magnets in a 10 TeV Muon Collider," Proceedings of 13th Int. Particle Acc. Conf., pp. 1671–1674, JACoW Publishing, Geneva, Switzerland, 7 2022, doi:10.18429/JACoW-IPAC2022-WEPOST001.

[18] R.J. Weggel et al., "Design Study for 20 T, 15 cm Bore Hybrid Magnet with Radiation-Resistant Insert for Pion Capture", Proc. of 2001 Part. Acc. Conf., pp 3398-3400, 2001.

[19] R.J. Weggel et al., "A Target Magnet System for a Muon Collider and Neutrino Factory", Proc. of 2nd Int. Part. Acc. Conf., pp 1650-1652, 2011.

[20] R.J. Weggel et al., "Magnet Design for the Target System of a Muon Collider/Neutrino Factory", Proc. of 5th Int. Part. Acc. Conf., pp 3976-3978, 2014, doi:10.18429/JACoW-IPAC2014-THPRI087.

[21] C. Accettura et al., "Conceptual Design of a Target and Capture Channel for a Muon Collider", IEEE TAS, 34(5), 2024, 4101705, doi:10.1109/TASC.2024.3368387.

[22] L. Bottura, et al., "Design and analysis of a HTS internally cooled cable for the Muon Collider target and capture solenoid magnets", accepted for publication in Cryogenics, 2024.

[23] Z.S Hartwig, et al., "VIPER: an industrially scalable high-current high-temperature superconductor cable", Supercond. Sci. Technol. 33 11LT01, doi:10.1088/1361-6668/abb8c0.

[24] D. Stratakis and R. Palmer, "Rectilinear six-dimensional ionization cooling channel for a muon collider: A theoretical and numerical study", Physical Review Special Topics-Accelerators and Beams, vol. 18, no. 3, p. 031003, 2015, doi:10.1103/PhysRevSTAB.18.031003.

[25] H.K. Sayed, R.B. Palmer and D. Neuffer, "High field–low energy muon ionization cooling channel", Physical Review Special Topics-Accelerators and Beams, vol. 18, no. 9, p. 091001, 2015, doi:10.1103/PhysRevSTAB.18.091001.

[26] R. Palmer, R. Fernow, and J. Lederman, “Muon collider final cooling in 30–50 T solenoids”, eConf. Proc. C110328, 2061 (2011).

[27] B. Bordini et al., “Conceptual design of a ReBCO non/metal- insulated ultra-high field solenoid for the Muon Collider”, 34(3), 2024, 4301310, doi:10.1109/TASC.2024.3361881.

[28] A. Molodyk, et al., “Development and large volume production of extremely high current density YBa2Cu3O7 superconducting wires for fusion”, Scientific Reports 11(1), 2021, doi:10.1038/s41598-021-81559-z.

[29] T. Mulder, et al. “Quench Protection of Stacks of No-Insulation HTS Pancake Coils by Capacitor Discharge”, IEEE TAS, 34(5), 2024, 4703906, doi:10.1109/TASC.2024.3362755.

[30] F. Batsch et al., “Longitudinal Beam Dynamics and RF Requirement for a Chain of Muon RCSs”, 14th Int. Particle Acc. Conf., 2023, doi:10.18429/JACoW-IPAC2023-TUPA040.

[31] A. Chancé et al., “Parameters Range for a Chain of Rapid Cycling Synchrotrons for a Muon Collider Complex”, Proceedings of 14th Int. Particle Acc. Conf., 2023,doi:10.18429/JACoW-IPAC2023-MOPL162.

[32] J.S. Berg and H. Witte, “Pulsed synchrotrons for very rapid acceleration,” in AIP Conference Proceedings, vol. 1777, p. 100002, AIP Publishing LLC, 2016, doi:10.1063/1.4965683.

[33] F. Boattini et al., “A Two Harmonics Circuit for the Powering of the Very Fast RCS (Rapid Cycling Synchrotron) of the Muon Collider Accelerator, 2023, Proceedings of 14th Int. Particle Acc. Conf., 2023, doi:10.18429/JACoW-IPAC2023-WEPM078.

[34] M. Breschi et al., “Comparative analysis of resistive dipole accelerator magnets for a Muon Collider”, IEEE TAS, 34(5), 2024, 4003305, doi:10.1109/TASC.2024.3360208.

[35] L. Rossi et al. “Design and plan of a 10 T HTS dipole for the Italian facility IRIS”, IEEE TAS, 34(5), 2024, 4602406, doi:10.1109/TASC.2024.3355357.

[36] H. Piekarz et al., “Record High Ramping Rates in HTS Based Superconducting Accelerator Magnet”, IEEE TAS, 32(6), 2022, 4100404.

[37] K. Skoufaris, C. Carli, D. Schulte, “10 TeV Center of Mass Energy Muon Collider, Proceedings of 13th Int. Particle Acc. Conf., 2022, doi:10.18429/JACoW-IPAC2022-MOPOTK031.

[38] Y.I. Alexahin, E. Barzi, E. Gianfelice-Wendt, Kapin et al., “Critical problems of energy frontier muon colliders: optics, magnets and radiation,” 2022, doi:10.48550/arXiv.2203.10431.

[39] V. Kashikhin,Y. Alexahin, N.V. Mokhov and A.V. Zlobin, “High-Field Combined-Function Magnets for a 1.5-1.5 TeV Muon Collider Storage Ring,” in Proc. 12th Int. Particle Acc. Conf., pp. 3587–3589, JACoW Publishing, Geneva, Switzerland.

[40] D. Novelli et al., "Analytical Evaluation of Dipole Performance Limits for a Muon Collider", IEEE TAS, 34(5), 2024, 4002405, doi:10.1109/TASC.2024.3352526.

[41] J.K. Hulm, R.D. Blaugher, Superconducting Solid Solution Alloys of the Transition Elements, Phys. Rev., 123(5) (1961) 1569, doi:10.1103/PhysRev.123.1569.

[42] B.T. Matthias et al., Superconductivity of Nb3Sn, Phys. Rev., 95(6) (1954) 1435, doi:10.1103/PhysRev.95.1435.

[43] E. Corenzwit, Superconductivity of Nb_3Al, J. Phys. Chem. Solids, 9(1) (1959) 93.

[44] Jun Nagamatsu, Norimasa Nakagawa, Takahiro Muranaka, Yuji Zenitani and Jun Akimitsu (1 March 2001). “Superconductivity at 39 K in magnesium diboride”, Nature 410 (6824): 63, doi:10.1038/35065039. PMID 11242039.

[45] M.K. Wu et al. Superconductivity at 93-K in a new Mixed-Phase Y-Ba-Cu-O Compound System at Ambient Pressure, Phys. Rev. Lett., 58 (9) (1987) 908, doi:10.1103/PhysRevLett.58.908.

[46] H. Maeda, Y. Tanaka, M. Fukutomi, and T. Asano, A New High-Tc Oxide Superconductor without a Rare Earth Element, Jpn. J. Appl. Phys. 27(2) (1988) L36l-4, doi:10.1143/JJAP.27.L209.

[47] Y. Kamihara, T. Watanabe, M. Hirano, H. Hosono, “Iron-based layered superconductor La O1-xFx FeAs (x=0.05-0.12) with $T_c = 26$ K”, J Am Chem Soc, 130 (2008), p. 3296, doi:10.1021/ja800073m.

[48] S. Carnot, “Réflexions sur la puissance motrice du feu et sur les machines propres à développer cette puissance”, Annales Scientifiques de l’É.N.S, 2e série, tome 1, 1872, p. 393-457, doi:10.24033/asens.88.

[49] A. Abada, et al., “FCC Physics Opportunities”, Eur. Phys. J. C 79, 2019, 474, doi:10.1140/epjc/s10052-019-6904-3.

[50] The CEPC-SPPC Study Group, “CEPC-SPPC Preliminary Conceptual Design Report”, IHEP-CEPC-DR-2015-01 (2018), doi:10.48550/arXiv.1809.00285.

[51] W. Abdallah et al., “CEPC Technical Design Report - Accelerator”, IHEP-CEPC-DR-2023-01, IHEP-AC-2023-01, 2023, doi:10.1007/s41605-024-00463-y.

[52] J. Tang, “Design Concept for a Future Super Proton-Proton Collider”, Front. Phys., Sec. Radiation Detectors and Imaging, 10, 2022, doi:10.3389/fphy.2022.828878.

[53] P. Lebrun & T. Taylor, "Managing the laboratory and large projects" in "Technology Meets Research, 60 years of CERN Technology: Selected Highlights", World Scientific (2017) p. 406.

[54] A. Abada et al., “FCC-hh: The Hadron Collider”, Eur. Phys. J. Spec. Top. 228, 2019, 755–1107, doi:10.1140/epjst/e2019-900087-0.

[55] L. Bottura, F. Zimmermann, “High energy LHC machine options in the LHC tunnel, in “The Future of the Large Hadron Collider”, O. Bruning, M. Klein, L. Rossi, P. Spagnolo Eds., World Scientific, 2024, 367-398, doi:10.1142/9789811280184_0026.

[56] L.D. Cooley, A.K. Ghosh, R.M. Scanlan, “Costs of high-field superconducting strands for particle accelerator magnets”, Supercond. Sci. Technol. 18(4), 2005, R51-R65, doi:10.1088/0953-2048/18/4/R01.

[57] V. Matias, R.H. Hammond, “YBCO superconductor wire based on IBAD-textured templates and RCE of YBCO: Process economics”, Physics Procedia, 36, 2012, 1440 – 1444, doi:10.1016/j.phpro.2012.06.239.